Aeroacoustics Conferences
June 4-7, 2024, Rome, Italy
30th AIAA/CEAS Aeroacoustics Conference (2024)

10.2514/6.2024-3258

An extensive near-field noise prediction of a subsonic jet using data-driven surrogate model based on neural networks

S. Meloni*
Università della Tuscia, Viterbo, Italy

F. Centracchio†, R. Camussi‡, U. Iemma§
Università degli Studi Roma Tre, Rome, Italy

G. Palma¶
CNR-INM, National Research Council, Institute of Marine Engineering

C. Bogey‖
CNRS, Ecole Centrale de Lyon, INSA Lyon, Université Claude Bernard Lyon I, Ecully, France

The use of surrogate models has become essential in modern design processes, with machine learning algorithms increasingly adapting to active metamodelling techniques. In this specific investigation, the formulation focuses on Artificial Neural Networks (ANNs) as data-driven nonlinear models. Within this study, ANNs formulation is used as a data–driven nonlinear model aimed at describing the dynamics and the noise emitted by a single-stream subsonic jet, trained with a large numerical database that includes a wide range of parameters. What sets this model apart is its pioneering incorporation of variables such as nozzle exhaust turbulence intensity and nozzle–exhaust boundary–layer thickness. These parameters significantly influence noise emissions and are challenging to model using traditional analytical methods. The training dataset was formulated using 80% of the information sourced from the numerical database derived from large-eddy simulations (LESs) of a jet flow operating at M=0.9 and $Re = 10^5$. Pressure time series were gathered from virtual probes placed at various radial and axial positions within the near field. The model has been properly validated and it is shown to predict well the pressure spectra over the entire range of frequencies of interest.

Nomenclature

x	=	axial distance from the nozzle exhaust
r	=	radial distance from the jet centerline
D	=	nozzle exhaust diameter
Re_D	=	nozzle exhaust Reynolds number. $Re_D = \rho U D/\mu$
St_D	=	Strouhal number. $St_D = fD/U$
U_j	=	nozzle exhaust jet velocity
M_j	=	jet Mach number
δ_{BL}	=	nozzle exhaust boundary layer

*Assistant Professor, Department of Economics, Engineering, Society and Business Organization, 01100 Viterbo, Italy, stefano.meloni@unitus.it, AIAA member

†Postdoctoral researcher, Department of Civil, Computer Science and Aeronautical Technologies Engineering, Via della Vasca Navale 79, 00146 Rome, Italy, francesco.centracchio@uniroma3.it, AIAA member

‡Full Professor, Department of Civil, Computer Science and Aeronautical Technologies Engineering, Via della Vasca Navale 79, 00146 Rome, Italy, roberto.camussi@uniroma3.it, AIAA member

§Full Professor, Department of Civil, Computer Science and Aeronautical Technologies Engineering, Via della Vasca Navale 79, 00146 Rome, Italy, umberto.iemma@uniroma3.it, AIAA member

¶Research scientist, CNR-INM, National Research Council, Institute of Marine Engineering, Via di Valeerano 139, 00128 Rome, Italy, giorgio.palma@cnr.it, AIAA member

‖CNRS Research Director, Laboratoire de Mécanique des Fluides et d'Acoustique, UMR 5509, Ecully, France, christophe.bogey@ec-lyon.fr, AIAA Associate Fellow

TI = Turbulence Intensity
r_0 = Jet radius
SPL = Sound Pressure Level
PSD = Power Spectral Density
ANN = Artificial Neural Networks
LES = Large Eddie Simulation
Var = Variance
$RMSE$ = Root-Mean-Square Error

I. Introduction

Jet noise is a long-standing issue in aviation due to its significant impact on the community. Because of ever-tightening noise regulations, the imperative to develop advanced strategies for mitigating jet engine noise is pressing. Contemporary commercial aircraft design needs the inclusion of acoustic emission considerations right from the initial concept stage. Thus, the development of rapid and dependable prediction methods holds pivotal importance in this domain.

Following existing literature, the near-acoustic field is defined by relatively small pressure fluctuations, allowing for linearization. The identification of coherent structures revolutionized the understanding of jet noise, paving the way for the introduction of the wave-packet approach [1–3], which is characterized by the involvement of modulating travelling waves. Several researchers have adopted and applied this method extensively to characterize and model jet noise sources [4]. However, due to proximity to the jet flow, the near-field fluctuations might be influenced by the rotational hydrodynamic pressure field. Within this zone, the predominant kinetic energy of fluctuations is associated with coherent structures along the azimuth, contributing to nonlinear effects in the evolution of wave packets [5]. Hence, considering the highlighted complexity, accurately predicting the noise source of high subsonic jets remains a challenging task.

In this framework, the principal focus of the present work is to present a data–driven metamodel capable of predicting the jet near-field noise. This metamodel aims to predict the near-field noise spectra generated by a subsonic jet, incorporating as a key parameter the initial conditions at the nozzle exhaust, such as turbulence intensity and boundary–layer thickness. The surrogate model developed herein is based on Artificial Neural Networks (ANNs), which represent a versatile tool that can be used to represent phenomena when their derivation and solution may be too cumbersome. The dichotomy between biological neurons and mathematical processes has been investigated in the 1940s [6, 7], but the theoretical layout of complex multilayer structures has been developed within the last 50 years [8, 9], thanks to the increase in computing resources. In order to manage the intrinsic complexity and richness of the jet near pressure field, the strategy we follow relies on the use of suitable surrogate models based on artificial intelligence techniques. Thus, the main focus is on leveraging the ANN-based approach to forecast jet noise spectra, while predicting uncertainty. Artificial neural networks are nowadays applied extensively also in fluid mechanics. Kim and Lee [10], for example, used the ANNs with a deep learning approach based only on wall information to predict turbulent heat transfer. In the work of Lee and You [11], the unsteady flow fields over a circular cylinder are used for training four different deep learning networks providing reliable predictions. Le Clainche et al. [12] presented a data-driven model applied to approximate the statistics of the averaged wall-shear stress in a turbulent channel flow over a porous wall. Centracchio et al. [13] recently proposed a data-driven nonlinear model based on ANNs to describe and predict the noise emitted by a single stream jet in under-expanded conditions. A metamodel on the wall pressure fluctuations generated by an installed supersonic jet has been carried out by Meloni et al. [14], Iemma et al. [15], while the prediction of the noise directivity generated by an ingesting boundary layer propeller has been presented by Meloni et al. [16]. Machine learning has been successfully exploited in similar configurations, for example, to correlate computational fluid dynamics data to the jet acoustic response [17] or to successfully predict the far-field noise spectra produced by supersonic jets with different nozzle shapes located near a surface [18].

Following the approach presented in Meloni et al. [14], we aim at providing a prediction of the sound pressure level with a low uncertainty in a large numerical domain which spans from the nozzle exhaust up to $x/D = 20$ in the streamwise direction and up to $r/D = 3$ in the radial direction. To tune the present model, we used a numerical dataset obtained from the Large-Eddy Simulation (LES) of an isothermal round free jet at a Mach number of 0.9 and a diameter-based Reynolds number of $Re_D = 10^5$ varying the nozzle-exhaust turbulence level between $TI = 0\%$ (fully laminar flow) and $TI = 15\%$, which is representative of a fully turbulent jet, and the boundary layer thickness at the nozzle exit between $\delta_{BL} = 0.05\, r_0$ and $\delta_{BL} = 0.4\, r_0$, where r_0 is the jet radius. The training data set contains pressure data at different axial and radial locations from $x/D = 0$ to $x/D = 20$ in the axial direction and from $r/D = 0.5$ to

$r/D = 3$ in the radial direction, respectively.

The remainder of the paper is organised as follows. Details on the numerical setup are given in Sec. II. Section III contains a brief description of the in-house dynamic ANN metamodel used in this work. Results and the model assessment with the uncertainty evaluation is included in Sec. IV whereas final remarks are given in Sec. V.

II. Numerical Setup

Large Eddy Simulations of round free jets at a Reynolds number $Re = 10^5$ and M=0.9 have been used for the analysis reported in this paper. The first set of LES considers jets with a nozzle–exhaust boundary–layer thickness fixed at $\delta_{BL} = 0.15 r_0$. The nozzle exit turbulence intensity has been varied in all the simulations with a step of $\Delta TI = 3\%$, starting from a fully laminar case with $TI = 0\%$ to the fully turbulent case $TI = 15\%$. These conditions have been achieved by tripping the pipe boundary layers using random low-level vortical disturbances decorrelated in the azimuthal direction. A second set of simulations has been carried out with $TI = 0$ and a normalized boundary–layer thickness δ_{BL}/r_0 varying from 0.025 up to 0.4 doubling the value of δ_{BL}/r_0 at each step.

For the sake of clarity, the jet initial conditions are summarized in Tab. 1.

Table 1 Jet initial conditions

M	0.9	0.9	0.9	0.9	0.9	0.9	0.9	0.9	0.9	0.9	0.9
Re_D	10^5	10^5	10^5	10^5	10^5	10^5	10^5	10^5	10^5	10^5	10^5
TI	0%	3%	6%	9%	12%	15%	0%	0%	0%	0%	0%
δ_{BL}/r_0	0.15	0.15	0.15	0.15	0.15	0.15	0.025	0.05	0.10	0.20	0.40

An in-house solver, based on the three-dimensional filtered compressible Navier–Stokes equations in cylindrical coordinates, has been used to perform the LES simulations. Specifically, the LESs were carried out using grids containing a number of points varying between 250 million and 1 billion, with low-dissipation schemes and relaxation filtering as a sub-grid dissipation model [19]. More useful details on the LES can be found in [5, 20–23].

The present study is limited to the near-field domain, usually identified as the noise-producing region of the jet flow and thus of interest for jet–noise modelling. Pressure time series are extracted from virtual probes at different locations in the near field, covering a domain that spans from the nozzle exhaust up to $x/D = 20$ in the axial direction and from the nozzle lip line ($r/D = 0.5$) up to $r/D = 3$ in the radial direction. The data set has been acquired at a sampling Strouhal number corresponding to $St = 12.8$ for 3221 time snapshots (see Fig. 1).

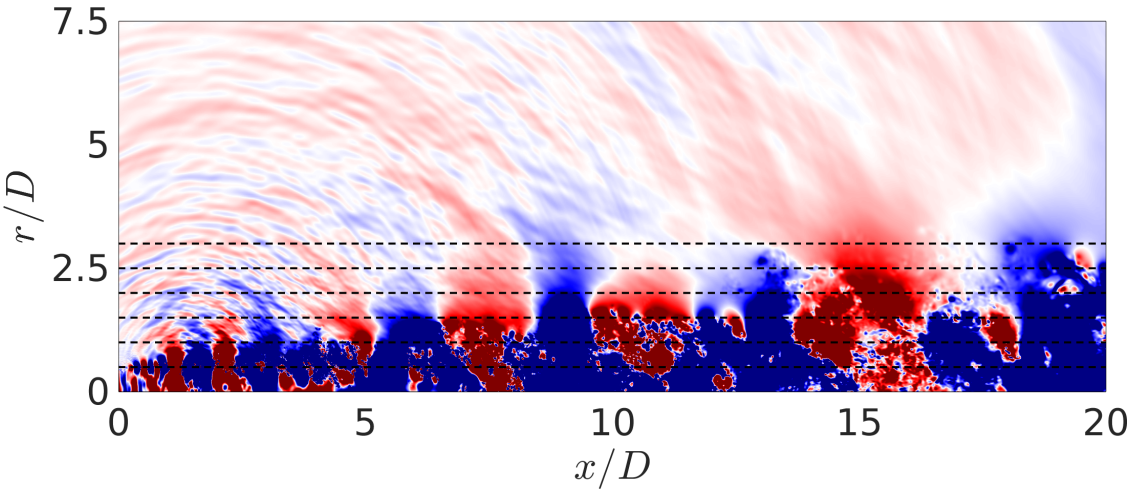

Fig. 1 Snapshot in the (x,r) plane of the pressure signals. The black dashed lines represent the probe arrays in the near field.

III. Neural Network Metamodel and Uncertainty

The ANN model consists of a group of information connections made up of artificial neurons: the elementary unit is the *perceptron*, a mathematical function that accepts several inputs and retrieve a single output. In the feed-forward, fully-connected architecture, the network is capable of receiving external signals on a layer of processing units (input nodes), each of which is connected with several inner nodes, organized in different layers: each node processes the received signals and transmits the result to subsequent nodes. In compact form, the output of the l-th layer, with $2 \leq l \leq L$ can be written as it follows

$$\mathbf{a}_l = \mathbf{f}_l \left(\mathbf{W}_{l\text{-}1} \mathbf{a}_{l\text{-}1} + \mathbf{b}_l \right) \tag{1}$$

so that the inputs $\mathbf{x} \equiv \mathbf{a}_1$ and the outputs $\mathbf{y} \equiv \mathbf{a}_L$. A schematic representation of a neural network is shown in Fig. 2.

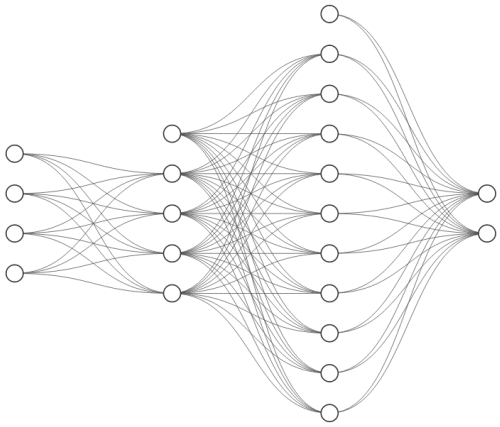

Fig. 2 Schematic representation of a neural network with 4 input nodes, two hidden layers (4 and 10 nodes respectively, with bias units) and 2 output nodes.

The selection of weight matrices $\{\mathbf{W}_l\}_{l=1}^{L\text{-}1}$ and bias vectors $\{\mathbf{b}_l\}_{l=2}^{L}$ is performed by means of the so–called *learning*, and is here addressed through the so–called *training with back-propagation* method: a cost function is computed at the t-th epoch (the iteration of the training process), so that its gradient is used to update weight and bias values, back-propagating the error information layer by layer [14]. Weights and biases at the t-th epoch are updated used the *learning rate*, a free parameter selected by the designer to control the change in weights and biases based on the error gradient components. As a result of the training process, the model can be completely identified by the parameters vector $\Theta = \{\mathbf{f}_l, \mathbf{W}_{l\text{-}1}, \mathbf{b}_l\}_{l=2}^{L}$, where $L = Q + 2$ and Q is the number of hidden layers.

The choice of the network topology and the selection of the parameters that regulate the training, represents a serious challenge given that they are significantly problem dependent. To overcome the issue, a suitable hyperparameter self–tuning coupled with a fully–deterministic topology optimisation scheme has been used here to derive the metamodel. Several rules have been implemented to address a data–informed tuning of the *training parameters* (weights and biases initialization, number of training epochs, batch size and learning rate), which affect the learning capability of the network. As the ANN fitting capability is sensitive to the *architectural parameters* (activation functions, number of hidden layers and number of neurons per layer), an in-house deterministic optimisation algorithm has been implemented.

The developed active metamodel is coupled with the quantification of its uncertainty. To this aim, the ANN response is assumed to be the expectation of a posterior continuous uniform probability $\mathcal{U}_j(\mathbf{x}) = \text{unif}\left\{a_j(\mathbf{x}); b_j(\mathbf{x})\right\}$ with $a_j(\mathbf{x}) < b_j(\mathbf{x})$. The hypothesis of continuous uniform distribution yields to the following definition of uncertainty related to the j-th component of the output vector

$$u_j(\mathbf{x}) = b_j(\mathbf{x}) - a_j(\mathbf{x}) = 2\sqrt{3}\sigma_j(\mathbf{x}) \tag{2}$$

being $\sigma_j = \sqrt{\text{Var}\left[\mathcal{U}_j(\mathbf{x})\right]}$ the standard deviation (here modelled with spatial correlation function). The metamodel global uncertainty $U(\mathbf{x})$ is evaluated as the normalised norm on the $\mathbb{R}^N$ Euclidean space

$$U(\mathbf{x}) = \sqrt{\frac{1}{N} \sum_{j=1}^{N} u_j^2(\mathbf{x})} \tag{3}$$

being $u_j(\mathbf{x})$ the magnitude of the uncertainty function of the j-th output. The uncertainty quantification allows for the implementation of adaptive sampling schemes aimed at driving the designer towards the choice of new experiments or simulations. Indeed, new a training point to be analysed can correspond to the maximum value of $U(\mathbf{x})$ as it follows

$$\mathbf{x}_{new} = \arg\max_{\mathbf{x}\in\mathcal{D}} [U(\mathbf{x})] \tag{4}$$

so that the size of the training set is systematically increased, and a new network can be built using the scheme described above.

IV. Results

To the extent of the noise level estimations, the Sound Pressure Level (SPL) was calculated as reported in the following equation:

$$SPL = 10\log_{10}\left(\frac{\mathrm{PSD}\Delta f_{\mathrm{ref}}}{P_{\mathrm{ref}}^2}\right), \tag{5}$$

where PSD denotes the power spectral density evaluated using Welch's method, Δf_{ref} is the frequency bandwidth and P_{ref} is the reference pressure in air (equal to 20μPa). Spectra have been represented in $1/3$–octave bands. The rationale underlying this choice lies in the fact that most aircraft noise prediction tools widely used in the aircraft design process make use of the $1/3$–octave bands description of the pressure signals. In addition, using band representation considerably reduces the number of training set data, resulting in faster network training.

Due to the specific arrangement of the data from the numerical simulations, two different databases have been created, the first one includes the data for different turbulence intensities and the second one accounts for data for different nozzle–exhaust boundary–layer thickness, each database is composed by 3 independent variables (x/D, r/D and TI for the first one and x/D, r/d and δ_{BL}/r_0 for the second one) associated with the 22 components of the SPL spectrum (related to the centre frequencies of the $1/3$–octave bands). In this view, two separate models of the vector collecting the $1/3$–octave bands SPL have been built. The first model provides the SPL as a function of x/D and r/D and δ_{BL}/r_0:

$$\begin{bmatrix} SPL_1 \\ \vdots \\ SPL_{\mathrm{N}} \end{bmatrix} = \mathbf{f}\left(\frac{x}{D}, \frac{r}{D}, \frac{\delta_{BL}}{r_0}\right) \tag{6}$$

In the second model, the independent variables are x/D and r/D and the TI percentage in the nozzle–exit turbulence level:

$$\begin{bmatrix} SPL_1 \\ \vdots \\ SPL_{\mathrm{N}} \end{bmatrix} = \mathbf{f}\left(\frac{x}{D}, \frac{r}{D}, TI_{\%}\right) \tag{7}$$

Both the datasets have been divided into two subsets: the 80% of the data was used as the training set $\mathcal{T}$ whereas 20% as a validation set $\mathcal{V}$. A fixed-budget architecture optimisation (consisting of 1000 objective function evaluations) has been performed for both the models. The characteristics of the optimal models are reported in Tab. 2, highlighting the characteristics of the final topology of the neural network with the activation functions.

Table 2 ANN final configuration related to both the BL and TI models.

	BL	TI
Optimal topology	3/14/23/20/22	3/32/37/22
Hidden layer activation	*swish*	*sinc*
Output layer activation	*sech*	*sigmoid*
$\mathrm{RMSE}_{\mathcal{T}}$	~2.5%	~2.5%
$\mathrm{RMSE}_{\mathcal{V}}$	<5%	<5%

It is interesting to highlight that, as shown in Tab. 2, the architecture optimisation process resulted in nearly identical training and validation losses for both the models. The convergence of root mean square error on the training set ($\text{RMSE}_{\mathcal{T}}$) as a function of the objective function evaluations is depicted in Fig. 3.

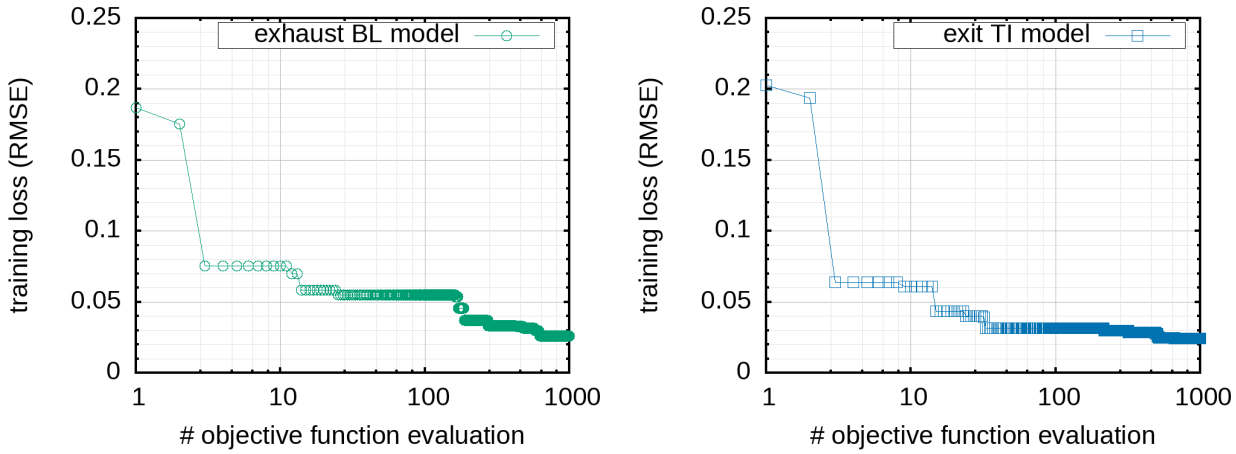

(a) (b)

Fig. 3 Convergence of $\text{RMSE}_{\mathcal{T}}$ as a function of the objective function evaluations for the BL (a) and TI (b) models.

Each data point of Fig. 3(a) and (b) corresponds to a unique neural network architecture, with its associated training loss value reflected on the given axis. It is worth highlighting than the architecture optimisation provided an improvement of about one order of magnitude in terms of training loss with respect to the training RMSE related to the first architectures analysed.

Figures 4 and 5 show the comparison between the responses of both models with the original data at different known locations.

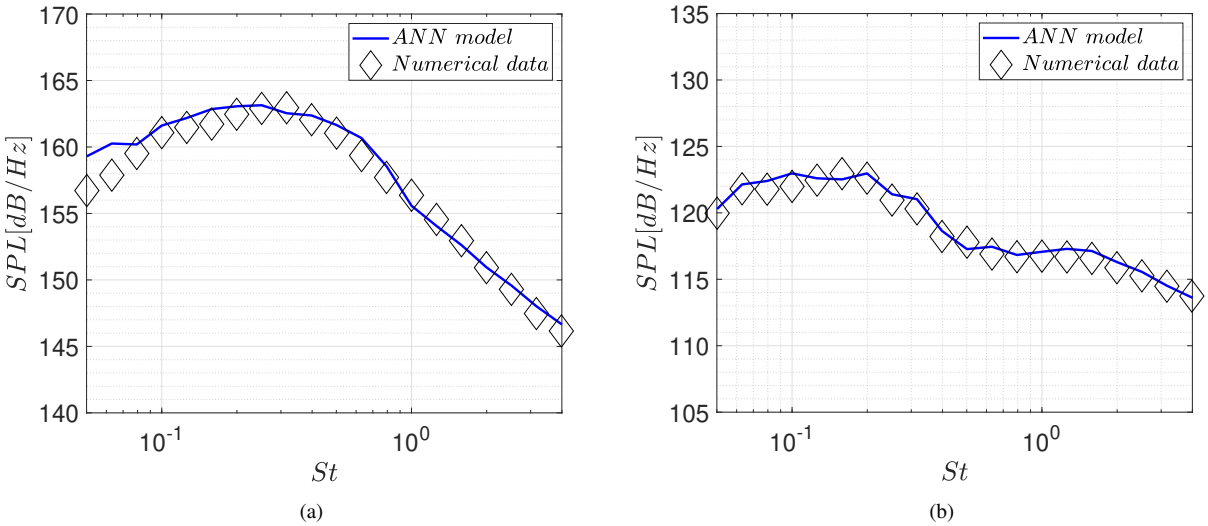

(a) (b)

Fig. 4 Comparison between turbulence intensity ANN metamodel response and original data at different known locations: (a) at x/D=1, r/D=0.5 and TI=15, (b) at x/D=17, r/D=0.5 and TI=9.

The analysis of Fig. 5 demonstrates that both ANN models align closely with the numerical data, effectively

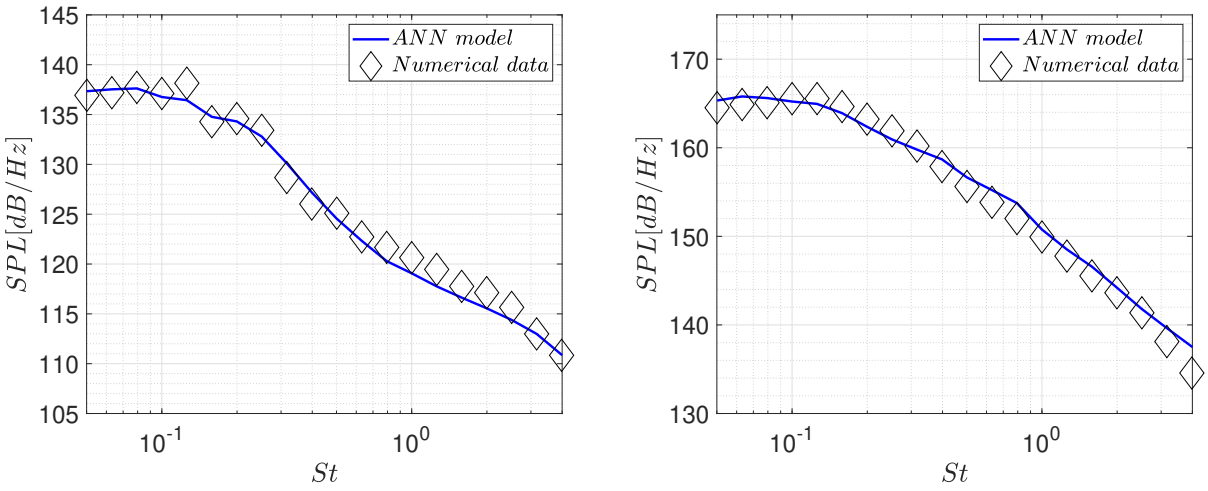

Fig. 5 Comparison between boundary layer thickness ANN metamodel response and original data at different known locations. (a) at x/D=1, r/D=1.5 and BL=0.025, (b) at x/D=18, r/D=1 and δ_{BL}/r_0=0.2.

reproducing the spectrum across a wide range of Strouhal numbers. Minor discrepancies are noted at the highest and lowest Strouhal numbers in both models, likely due to these points being situated near the models' boundaries. Figures 6 and 7 illustrate the model's responses in terms of SPL at different radial and axial locations.

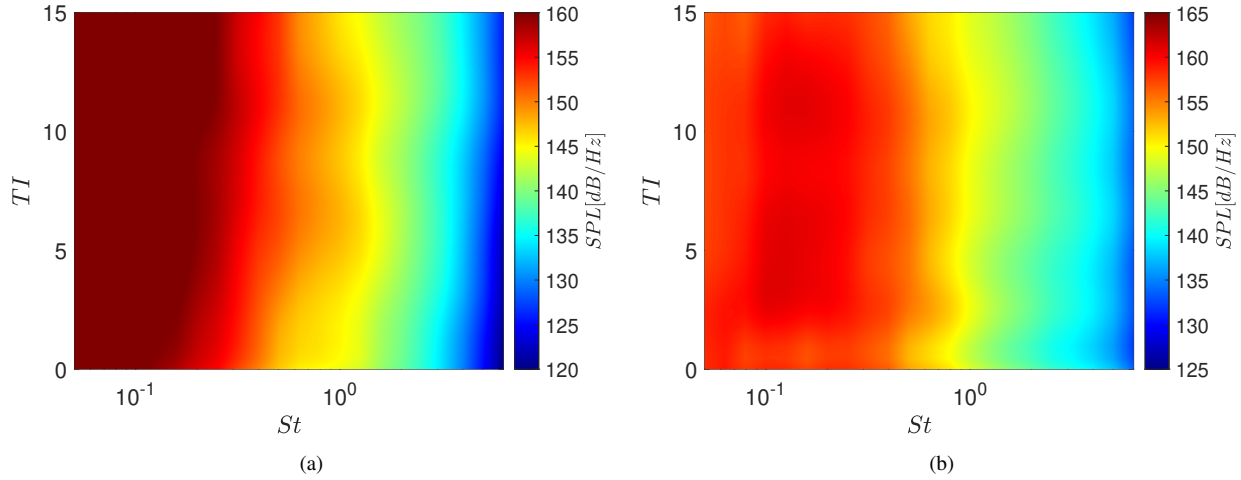

Fig. 6 ANN metamodel response for different TI: (a) at x/D=8 and r/D=2, (b) at x/D=16 and r/D=1.2.

According to the literature, an increase in turbulence intensity leads to a notable increase in noise levels, particularly at lower frequencies and closer to the nozzle exhaust this is observed in Fig. 6. This effect is more pronounced at lower values of turbulence intensity. On the other hand, Fig. 7 shows that the noise increase is primarily due to the thickness of the boundary layer near the nozzle exhaust. This observation highlights the importance of considering boundary–layer effects when analyzing the model's response.

It is crucial to emphasize that a proper quantification of the model's uncertainty is essential for estimating the reliability of its predictions. The ANN model uncertainty maps of both models are reported Fig. 8 and Fig. 9 covering almost the whole domain.

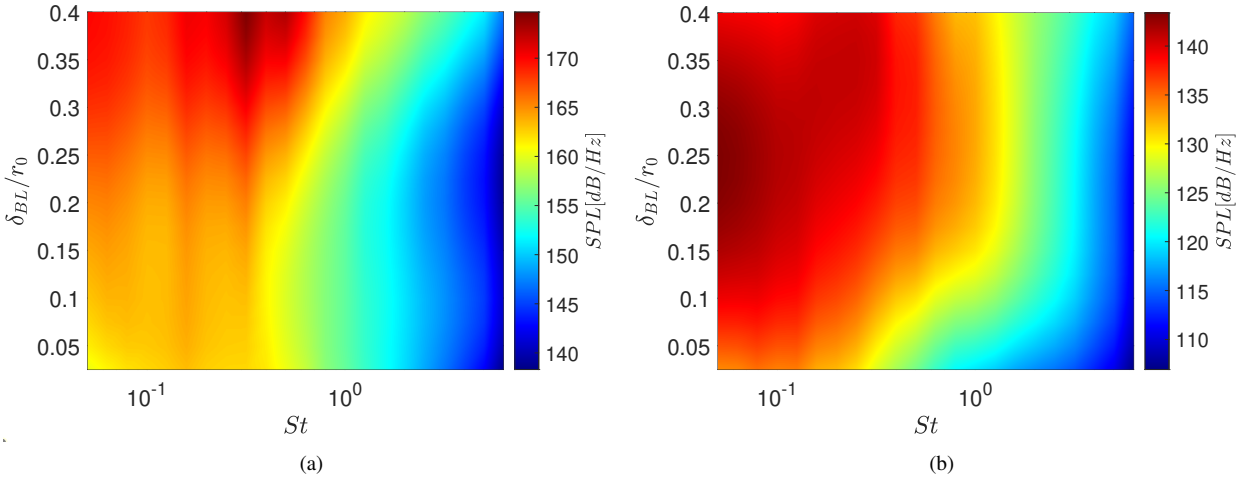

(a) (b)

Fig. 7 ANN metamodel response for different BL: (a) at x/D=4 and r/D=1.3, (b)x/D=15 and r/D=2.

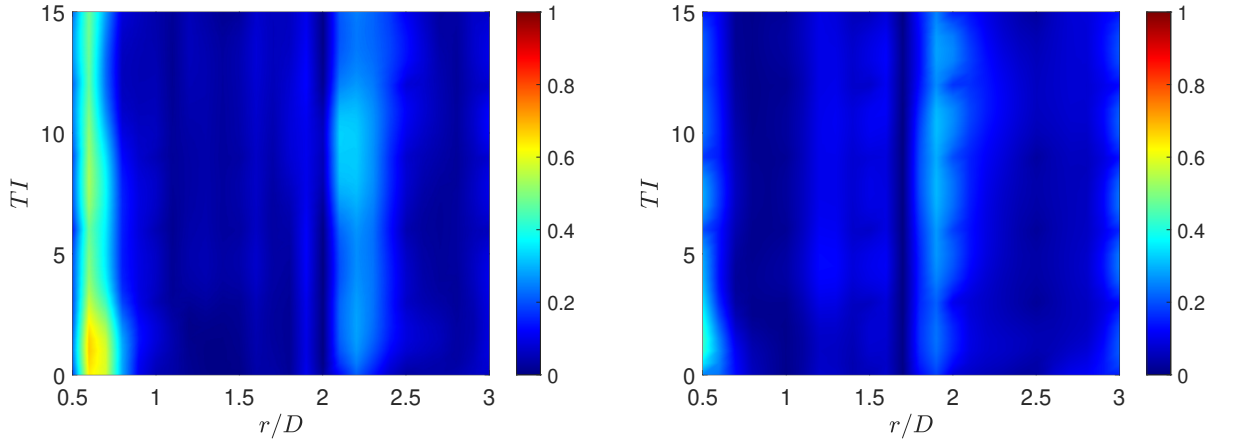

(a) (b)

Fig. 8 ANN metamodel uncertainty for different nozzle–exhaust turbulence intensities and different radial distances: (a) at x/D=6.5 and (b) at x/D=19.

It can be observed that both models show low uncertainty values across most of the domain. Analyzing Fig. 8(a) in detail, high uncertainty values can be observed near the jet plume (low r/D), distributed evenly across the different turbulence levels. This behaviour may be correlated with the strong variation of the spectra in that area due to the very strong aerodynamic fluctuations at $r/D = 0.5$. This uncertainty signature disappears at high x/D values in Fig. 8(b), likely due to the development of the jet turbulence, which reduces the differences between the spectra. Low uncertainty has also been observed for the boundary layer thickness model, especially at high x/D values in Fig. 8(b). In the uncertainty map for the area closest to the jet exit Fig. 8(a), this model also exhibits signatures with higher uncertainty values. These are mostly located between δ_{BL}/r_0=0.2 and δ_{BL}/r_0=0.4 due to the sparse number of training points in this area.

In conclusion, the uncertainty graphs highlight the need to train the model with a greater number of data points near the jet plume and higher boundary layer thicknesses.

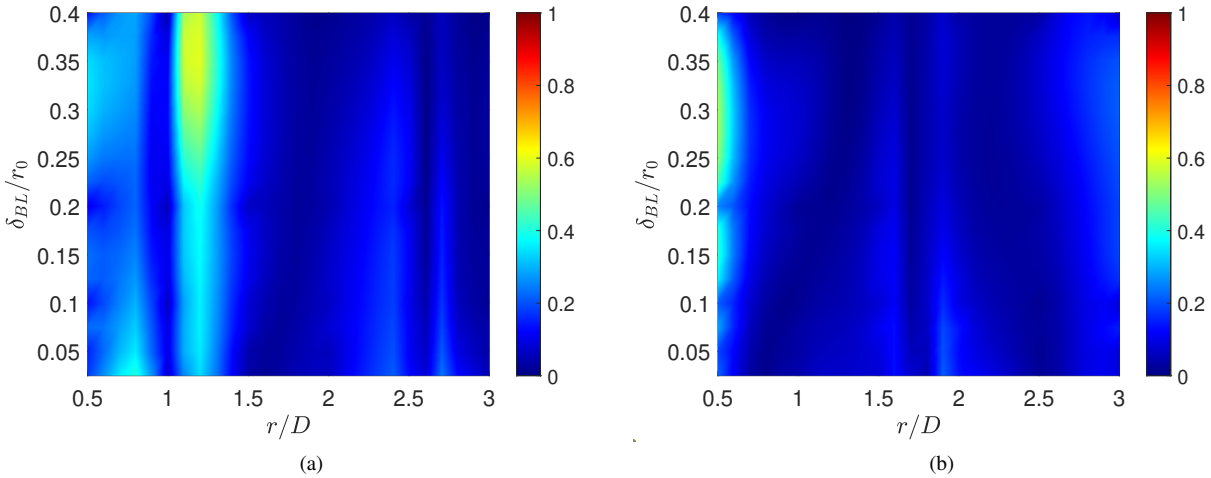

Fig. 9 ANN metamodel uncertainty for different boundary layer thicknesses and different radial distances: (a) at x/D= 4.5 and (b) at x/D=19.5.

V. Concluding Remarks

The present paper outlines the development of an Artificial Neural Network (ANN) metamodel, meticulously trained on a large numerical dataset to the scope of predicting the near-field noise of a jet under different initial conditions. A fully deterministic architecture optimization algorithm has been used to derive the ANN topology and the activation functions combination. The algorithm is coupled with a suitable self-tuning scheme to select the network training parameters. As expected, the accuracy of the prediction depends on the number of iterations. In the application presented here, a training set error less than 2.5% (with a validation error of approximately 5%) steps. The main physical parameters considered at the nozzle exit are the turbulence level and the boundary–layer thickness. Two distinct ANN models are built to reproduce the influence of the two parameters upon the near field pressure fluctuations. It is shown that both models effectively capture the dynamics of the data, providing predictions consistent with expected physical behavior. The analysis confirms that both ANN models closely match the numerical data, accurately replicating the spectrum over a broad range of Strouhal numbers. Both models exhibit low uncertainty across most of the domain, emphasizing the importance of training the models with a large number of data points near the jet plume and for large boundary–layer thickness.

Acknowledgments

This work has been supported by the European Union's Horizon 2020 research and innovation program under project ENODISE (enabling optimized disruptive airframe-propulsion integration concepts), grant agreement no. 860103.

C. Bogey was partially supported by the LABEX CeLyA (ANR-10-LABX-0060/ANR-16-IDEX-0005). The numerical data analyzed in this work were obtained using the HPC resources of PMCS2I (Pôle de Modélisation et de Calcul en Sciences de l'Ingénieur et de l'Information) of Ecole Centrale de Lyon and P2CHPD (Pôle de Calcul Hautes Performances Dédié) of Université Lyon I, and the resources of CINES (Centre Informatique National de l'Enseignement Supérieur) and IDRIS (Institut du Développement et des Ressources en Informatique Scientifique) under the allocation 2021-2a0204 made by GENCI (Grand Equipement National de Calcul Intensif).

References

[1] Jordan, P., and Colonius, T., "Wave Packets and Turbulent Jet Noise," *Annual Review of Fluid Mechanics*, Vol. 45, No. 1, 2013, pp. 173–195. https://doi.org/10.1146/annurev-fluid-011212-140756.

[2] Rodríguez, D., Jotkar, M. R., and Gennaro, E. M., "Wavepacket models for subsonic twin jets using 3d parabolized stability equations," *Comptes Rendus Mécanique*, Vol. 346, No. 10, 2018, pp. 890–902.

[3] Sandham, N., Morfey, C., and Hu, Z., "Sound radiation from exponentially growing and decaying surface waves," *Journal of Sound and Vibration*, Vol. 294, No. 1, 2006, pp. 355–361. https://doi.org/doi.org/10.1016/j.jsv.2005.10.012.

[4] Cavalieri, A. V. G., Jordan, P., Colonius, T., and Gervais, Y., "Axisymmetric superdirectivity in subsonic jets," *Journal of Fluid Mechanics*, Vol. 704, 2012, p. 388–420. https://doi.org/10.1017/jfm.2012.247.

[5] Palma, G., Meloni, S., Camussi, R., Iemma, U., and Bogey, C., "Data-Driven Multiobjective Optimization of Wave-Packets for Near-Field Subsonic Jet Noise," *AIAA Journal*, Vol. 61, No. 5, 2023, pp. 2179–2188. https://doi.org/10.2514/1.J062261.

[6] McCulloch, W., and Pitts, W., "A logical calculus of the ideas immanent in nervous activity," *The bulletin of mathematical biophysics*, Vol. 5, 1943, pp. 115–133. https://doi.org/10.1007/BF02478259.

[7] Hebb, D., *The Organization of Behaviour*, John Wiley & Sons, Inc., 1949.

[8] Ivakhnenko, A., *Cybernetics and forecasting techniques*, Elsevier Science Ltd, 1967.

[9] Ivakhnenko, A., *Cybernetic predicting devices*, CCM Information Corporation, 1973.

[10] Kim, J., and Lee, C., "Prediction of turbulent heat transfer using convolutional neural networks," *Journal of Fluid Mechanics*, Vol. 882, 2020, p. A18. https://doi.org/10.1017/jfm.2019.814.

[11] Lee, S., and You, D., "Data-driven prediction of unsteady flow over a circular cylinder using deep learning," *Journal of Fluid Mechanics*, Vol. 879, 2019, p. 217–254. https://doi.org/10.1017/jfm.2019.700.

[12] Le Clainche, S., Rosti, M., and Brandt, L., "A data-driven model based on modal decomposition: application to the turbulent channel flow over an anisotropic porous wall," *Journal of Fluid Mechanics*, Vol. 939, 2022, p. A5. https://doi.org/10.1017/jfm.2022.159.

[13] Centracchio, F., Meloni, S., Jawahar, H. K., Azarpeyvand, M., Camussi, R., and Iemma, U., "Under–expanded jet noise prediction using surrogate models based on artificial neural networks," *28th AIAA/CEAS Aeroacoustics Conference*, 2022. https://doi.org/10.2514/6.2022-3025.

[14] Meloni, S., Centracchio, F., de Paola, E., Camussi, R., and Iemma, U., "Experimental characterisation and data-driven modelling of unsteady wall pressure fields induced by a supersonic jet over a tangential flat plate," *Journal of Fluid Mechanics*, Vol. 958, 2023, p. A27. https://doi.org/10.1017/jfm.2023.84.

[15] Iemma, U., Centracchio, F., Meloni, S., and Camussi, R., "Artificial Neural Networks Metamodels Tailored To Jet Induced Wall Pressure Fluctuations," *28th International Congress on Sound and Vibration (ICSV 28)*, 2022. https://doi.org/10.2514/6.2022-3025.

[16] Meloni, S., Centracchio, F., Falsi, M., Zaman, I., Zang, B., Azarpeyvand, M., Iemma, U., and Camussi, R., "Data-driven model for the prediction of the noise emitted by a boundary layer ingesting propeller," 2023.

[17] Popov, V., Boust, F., and Burokur, S. N., "Constructing the Near field and Far field with Reactive Metagratings: Study on the Degrees of Freedom," *Phys. Rev. Appl.*, Vol. 11, 2019, p. 024074. https://doi.org/10.1103/PhysRevApplied.11.024074.

[18] Brown, C. A., Dowdall, J., Whiteaker, B., and McIntyre, L., *A Machine Learning Approach to Jet-Surface Interaction Noise Modeling*, 2020. https://doi.org/10.2514/6.2020-1728.

[19] Bogey, C., Marsden, O., and Bailly, C., "Large-eddy simulation of the flow and acoustic fields of a Reynolds number 10^5 subsonic jet with tripped exit boundary layers," *Physics of Fluids*, Vol. 23, 2011, p. 035104.

[20] Bogey, C., "Acoustic tones in the near-nozzle region of jets: characteristics and variations between Mach numbers 0.5 and 2," *Journal of Fluid Mechanics*, Vol. 921, A3, 2021. https://doi.org/10.1017/jfm.2021.426.

[21] Bogey, C., "Grid sensitivity of flow field and noise of high-Reynolds-number jets computed by large-eddy simulation," *International Journal of Aeroacoustics*, Vol. 17, No. 4-5, 2018, pp. 399–424. https://doi.org/10.1177/1475472X18778287.

[22] Bogey, C., "A database of flow and near pressure field signals obtained for subsonic and nearly ideally expanded supersonic free jets using large-eddy simulations," https://hal.archives-ouvertes.fr/hal-03626787, 2022.

[23] Camussi, R., Meloni, S., and Bogey, C., "On the influence of the nozzle exhaust initial conditions on the near field acoustic pressure," *Acta Acust.*, Vol. 6, 2022, p. 57. https://doi.org/10.1051/aacus/2022051.